

Development report of a G-APD based detector system for the new high-field spectrometer (Laboratory for Muon Spin Spectroscopy, PSI, Switzerland)

J. Rodriguez, R. Scheuermann, K. Sedlak, A. Stoykov and A. Amato
Paul Scherrer Institut, CH-5232 Villigen PSI, Switzerland

October 3, 2011

Abstract

We present the advances on the development of a detector system for the new high-field spectrometer in PSI based on the use of Geiger-mode Avalanche PhotoDiodes (G-APD).

1 Introduction

In the Muon Spin Rotation/Relaxation/Resonance (μ SR) technique, 100% polarized muons are implanted into the material under study. The muons decay with a half life of $2.19\mu\text{s}$ by emitting a positron preferentially along the muon spin direction. Then, by placing a set of detectors around the material, the polarization of the muon ensemble as a function of time can be found. This polarization contains important information about the magnetic and electronic properties of the material.

In the Laboratory for Muon Spin Spectroscopy (LMU) we are developing a new High Magnetic Field Spectrometer (HMFS) which will expand the range of the μ SR technique [1]. In this spectrometer μ SR materials will be studied in a temperature range from ≈ 20 mK to 375 K, and in magnetic fields up to 9.5 T. This high magnetic field imposes a very strong demand on the time resolution of the detector system. For instance, the reduction of the amplitude of the μ SR signal due to the finite time resolution of the detector system is given by [2]:

$$A = e^{-2(\pi\sigma\nu)^2} \quad (1)$$

where σ is the time resolution of the detector and ν is the frequency of the μ SR signal. In a traditional μ SR spectrometer the detector system has a time resolution $\sigma=425$ ps. This means that the amplitude of the μ SR signal at 9.5 T would be 0.3% and, therefore, undetectable. For the HMFS it has been specified that the amplitude of the μ SR signal should be about 0.5 at 9.5 T, and in consequence, the detector must have a time resolution better (*i.e.* smaller) than 140 ps.

Achieving the time resolution required by the HMFS requires new technological innovations. Traditional detector systems for μ SR spectrometers are based on photomultiplier tubes. This technology has two main problems: first, photomultiplier tubes can not operate in the presence of a large magnetic field; and second, they are bulky. The first problem is solved by placing the photomultiplier tubes far from the magnet and using waveguides to transport the light from the scintillators to them. This solution though, worsens the time resolution of the spectrometer. If a time resolution better than 140 ps is desired then a detector system without waveguides, where the detectors are located inside the field, is necessary.

We have performed Monte Carlo simulations of different experimental setups with the GEANT4 package in order to find optimum geometrical constraints for the HMFS detector system [3]. We found that, in order to keep a good performance of the spectrometer, the detectors should be located at a distance of 21mm from the sample (Figure 1 C). This imposes a further constrain in the detector system since it not only has to work in the presence of a magnetic field, it has to be compact.

The problems stated in the previous two paragraphs can be overcome if G-APD detectors are used instead of photomultiplier tubes. In the Laboratory for Muon Spin Spectroscopy (LMU) at the Paul Scherrer Institut (PSI) we have an ongoing program to develop new μ SR detectors based this technology. G-APD detectors are insensitive to magnetic fields and, since they are much more compact, they can be placed near the sample under study. Further more, since G-APD based detectors can be manufactured without magnetic components, they can be placed near the sample without disturbing the applied magnetic field. Also, G-APD based μ SR detectors perform very well when compared to those based on photomultiplier tubes. We have measured the best-attainable time resolution of a G-APD based setup as a function of the energy deposited in the scintillator. We have found that our results compete with the best results attained with photomultiplier tubes [4].

The HMFS will have two set of detectors, one for the dilution refrigerator (20 mK-30 K) and an other for the flow cryostat (<3K - 375 K). The timing part of the detector system for both units will consist of 16 positron counters arranged in two rings of forward and backward detectors (Figure 1A shows a sketch of the experimental setup with the 16 detectors). The diameter for these detector rings will be 42mm and 30mm for the Dilution Refrigerator (DR) and flow cryostat (FC) respectively. These values were specified after analyzing GEANT4 simulation of several experimental setups. Figure 1 B) shows that as the radius of the detector is increased, the amount of positrons that hit the detectors is also decreased. Nevertheless, as Figure 1 C) and D) shows, the figure of merit decreases slower than what Figure 1 B) would imply. This is because as the radius of the detector is increased, only more and more energetic positrons are able to reach the detectors (the others spiral out). These high energetic positrons are those which are most asymmetric and give larger amplitudes of the signal. The detector diameters for the DR and FC were determined considering Figure 1 C) and technological constrains. The veto part of the detector system will be located inside the units. The light from the veto counters of the DR (placed at the 1 K shield) will be delivered to the G-APD located outside by an optical extraction array (see Section 3); while that of the FC (mounted in the sample stick) by a set of wavelength-shifting optical fibers. The veto part of the detector will be in charge of muon and positron validation (this last one only for the DR).

In the remaining of this documents we show our most recent developments for the HMFS. In Section 2 we present the performance of two full detector prototypes, and in Section 3 we show the results from the first optical extraction system test.

2 Timing detector prototype

We have built and tested a timing detector prototype in magnetic fields up to 4.5T inside the ALC magnet at PSI. Figure 2 shows a picture of the prototype, and Figure 3 shows the internal details of the prototype. The timing detector consists of one muon counter and 16 positron counters arranged in two rings of backward and forward positron detectors. Each individual counter consists of a plastic scintillator, a photosensor constructed as a pair of G-APDs operated in series connection, a printed board used for mounting purposes, and an amplifier (not shown in the figures) connected to the board via a single ~ 20 cm long cable, supplying to the photosensor the bias voltage and taking out its signal. The test sample was introduced in the “sample holder” cavity (see Figure 3), which has a diameter of 29mm, and the temperature of the detector system was stabilized indirectly to 42°C by a heater attached to the sample stick.

To determine the time resolution of the detector we used a single crystal of quartz. In this material muonium formation produce several frequencies in the same signal for a given field. By extracting the amplitudes of these signals and scaling them by the appropriate polarizations [5], we obtained the amplitude as a function of frequency which is shown in Figure 4. The detector time resolution was found to be 90 ps in low fields, and 82n ps at high fields. If we subtract from this the contribution of the Time to Digital Converter, we get a time resolution of 75 ps at low fields and 65 ps at high fields. The observed improvement of the time resolution towards the high fields is presumably due to higher energy losses of positrons crossing the counters at more inclined trajectories. Both of these numbers are much lower than the limit of 140 ps set in the specifications of the high-field μ SR spectrometer.

More recently we have performed a preliminary test with this timing detector in the new 9.5 T magnet. Figure 5 shows the μ SR signal in a high purity silver sample. The large amplitude of the signal should be noted. Figure 5 also shows the Fourier transform of the signal.

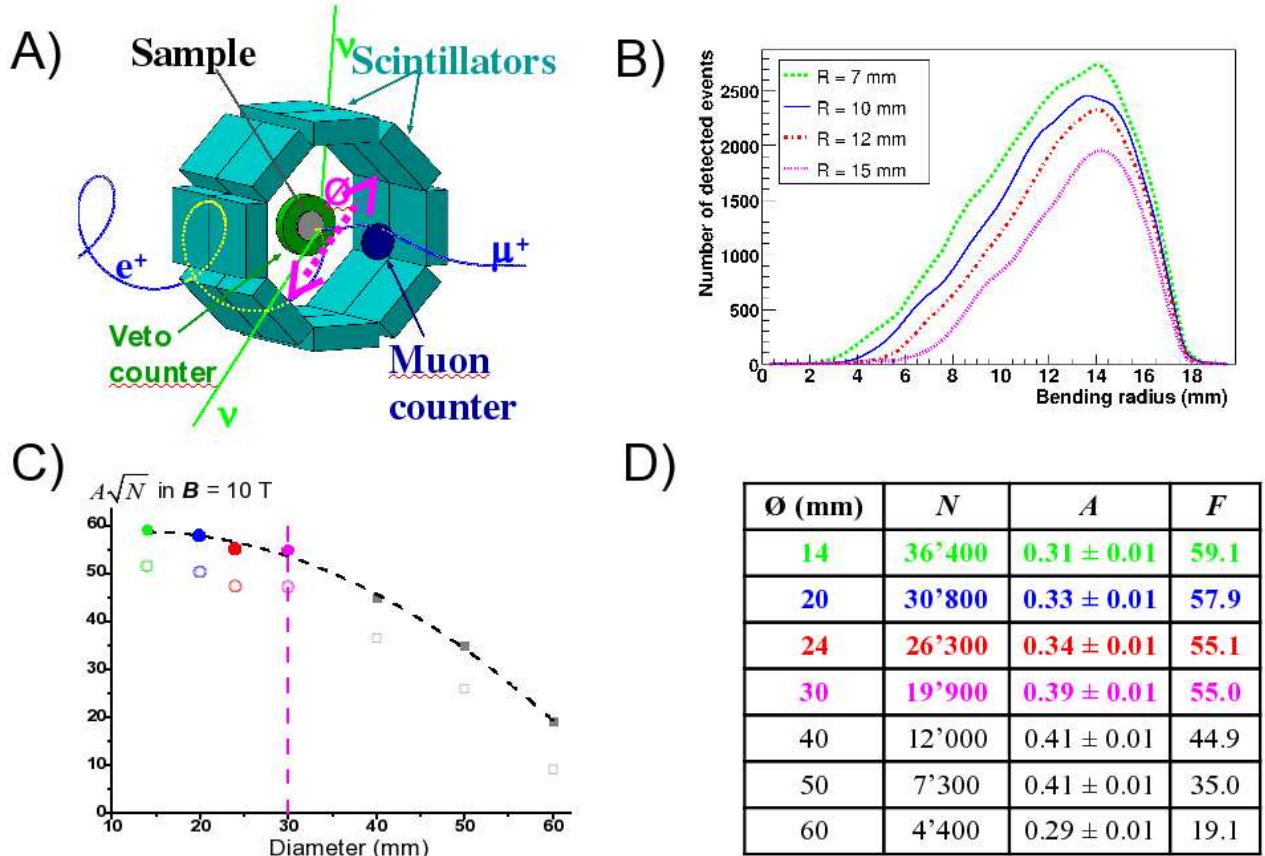


Figure 1: A) Sketch of the experimental setup which shows a simulated event (muon being implanted in the sample, and subsequent positron decay). The 16 detectors (sensitive volumes in GEANT4) are shown. B) Histogram of the number of positrons which arrived to the detectors in the GEANT4 simulation as a function of the bending radius ($r = P_t/Be$ where P_t is the transverse momentum of the positron at the moment of the decay and B the local magnetic field). C) Figure of merit at 10 T ($F = A\sqrt{N}$, where A is the simulated amplitude of the μ SR signal and N is the number of detected events) as a function of the radius of the detectors obtained with GEANT4. Note that for every simulated radius the solid angle of the detectors was kept constant. D) Table containing the radius of the detectors, the amplitude of the μ SR signal, the number of detected events and the figure of merit.



Figure 2: Prototype timing detector. The aluminized mylar window for incoming muons can be seen in the front of the detector. Only 4 positron counters and the muon counter have been wired in this picture

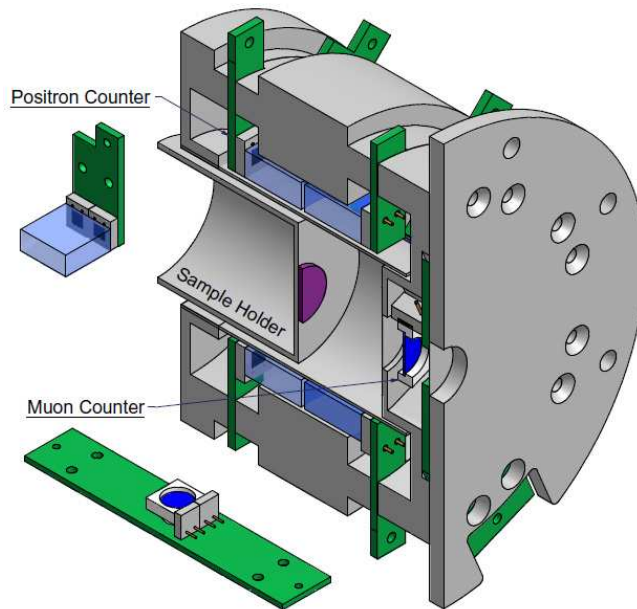


Figure 3: Prototype of the Timing detector module: design view. Plastic scintillators of type EJ-232 from Eljen are used. Their dimensions: $\varnothing 7 \times 0.3$ mm (muon counter), $12 \times 12 \times 5$ mm (positron counter). Each scintillator is readout by a pair of G-APDs of type MPPC S10362-33-050C from Hamamatsu Photonics.

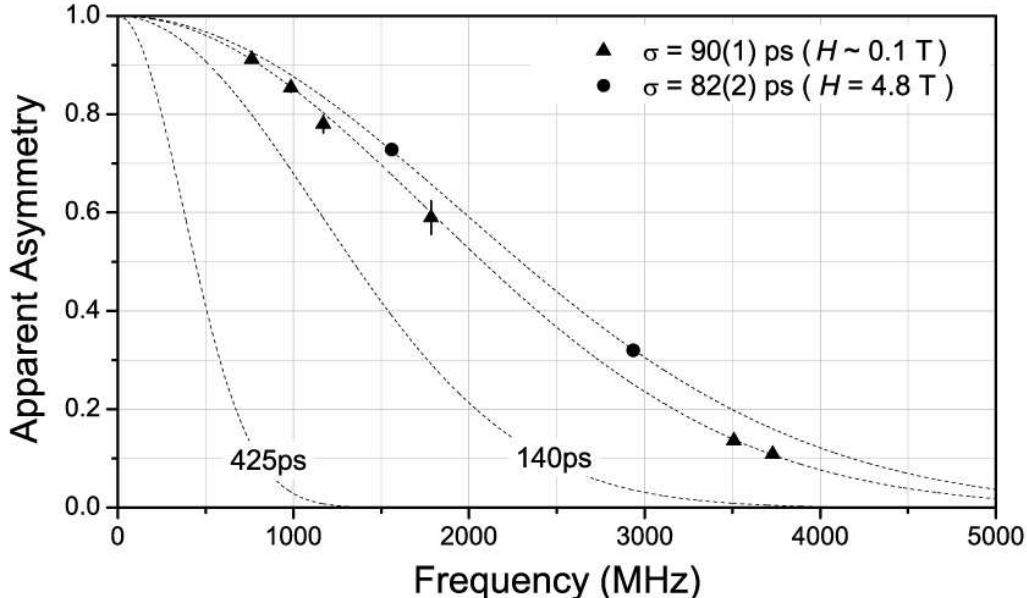


Figure 4: Reduction of the apparent muonium asymmetry $A_{\text{Mu}}(\nu)/A_{\text{Mu}}(0)$ with increasing the signal frequency measured on a synthetic quartz crystal in transverse magnetic fields of 0.07, 0.1, and 4.8 T. The dashed lines represent the dependence for different values of the time resolution. For comparison, Equation 1 is plotted for the a characteristic time resolution of a “standard” μSR instrument (~ 425 ps) and that expected for a spectrometer with a $\sigma = 140$ ps (the specified time resolution for the HMFS).

3 Optical extraction system for a G-APD based detector system

The veto part of the detector system has to be mounted inside the sample space in order to produce a proper muon a positron validation. For the DR a straightforward solution for veto signal extraction would be a continuous (presumably fiber) light guide going to the photosensor through the body of the cryostat. This, however, interferes with the foreseen DR design and is difficult to implement without compromises. An alternative solution is to collect the light from the fiber by an optical lens system and transport it through the shield of the DR tail also with an optical system.

Figure 6 outlines the layout of the detector system for the DR. The muon veto Mv and positron validation Pv detectors are located in the vicinity of the sample. Mv serves the purpose of additionally collimating the incoming muon beam: only those muons which pass through the central hole in this counter will be accepted by the data acquisition system. Pv works in coincidence with Pt: it confirms that a decay positron detected by Pt has originated from a small inner volume surrounded by Pv. GEANT4 simulations indicate that this scheme reduces the intensity of random Mt-Pt coincidences contributing to the uncorrelated background in the μSR spectra. The Pv detector has a cylindrical shape and is divided into 4 segments of independent scintillation counters to provide additional information about the direction at which a decay positron has been emitted. Due to space limitations we can not afford more than 5 mm thickness for a Pv counter (taking into account spiraling of the decay positrons in high magnetic fields, the diameter of the Pt detector ring, and accordingly the cryostat diameter, should be kept as small as possible [3]). Pv represents the most critical part in terms of ensuring the required performance: relativistic decay positrons passing through this counter deposit a factor of 3 less energy compared to 29 MeV/c muons stopping in Mv.

The elements of the optical array are shown in Figure 7. The R-Lens was built in two versions, depending on the active area of the photosensor to be used: the R-Lens-3 is used with a 3 x 3 mm² Hamamatsu MPPC S10362-33-050C [6], the stronger R-Lens-1 allows to focus the light onto a smaller device, a $\varnothing 1.1$ mm Photonique SSPM 0810G1MM [7]. Depending on which R-Lens is used, we will refer to the optical array as LLG-1 or LLG-3.

The coupling efficiency (CE) of LLG-3 was obtained in measurements with a 90 Sr radioactive source. The 3

x 3 mm² active area G-APD was coupled to the fiber either directly (no optical grease was used), or via the lens light guide. Comparing the signal amplitudes (their mean values) in both cases we obtain the CE of LLG-3 as 75% Direct coupling of \varnothing 1.1 mm G-APD to the fiber was not possible, since the last two elements of R-Lens-1 were glued onto it. Consequently, the coupling efficiency of LLG-1 was determined indirectly using a UV lamp and the known CE from LLG-3. We have estimated the CE of LLG-1 to be \approx 55%.

Even though the R-Lens system will be attached to the 1K shield, some relative displacement between the R-Lens and T-Lens system due to thermal contraction can be expected. It is desired then to quantify the sensitivity of LLG-1 and LLG-3. The signal amplitude at a displacement of \pm 2 mm of the T-lens from the R-lens was found to be 90% and 70% of its maximum value with the R-Lens-3 and R-Lens-1 respectively.

Thanks to the fact that the smaller active area G-APD used with LLG-1 has a factor of 2 lower noise level compared to the larger one used with LLG-3, the signal-to-noise ratio in the first case is a factor of 1.4 better, although the amount of collected light is smaller. Considering the insensitivity of the LLG-1 to the relative displacement of its transmitting and receiving lenses as acceptable, further tests in a cryogenic system were performed using this version of the lens light guide.

A cryogenic test is necessary for studying the thermal stability of the optical array. For this test we adapted the existing cryostat of the ALC μ SR spectrometer: both the outer vacuum chamber and the radiation shield were split into two parts a long (\sim 70 cm) base and a short (\sim 15 cm) removable front tail housing the detector. The tests were performed with a 29 MeV/c positron beam at the π E3 beamline in PSI. Figure 8 shows the details of the optical extraction array in the cryogenic test. We performed three cooling cycles of our system (from 300 K to 3 K the base temperature of our cryostat). For each new cycle the cooling and heating rates were increased. During the fastest cycle the cooling rate was not less than 3 K/min and the heating rate reached even 10 K/min. No problems with the mechanical stability of the system were encountered. During all cryogenic tests the performance of the detector has been stable with the signal-to-noise ratio well exceeding the acceptable level in the whole temperature range.

4 Conclusions

We have demonstrated the feasibility of a G-APD based detector system for the future HMFS at PSI. We have successfully implemented a timing detector prototype. We measured the time resolution of this detector to be 75 ps at low fields and 65 ps at high fields. This is much lower than the maximum value of 140 ps set in the specifications of the HMFS. Recently this detector was tested up to 9.5 T in the new high field magnet. The observed μ SR signals were observed to have big amplitudes and had sharp spectral lines. Also, we have built and tested a prototype for the optical extraction of the veto detector signal. This prototype showed good efficiency for signal transmission and was mechanically stable from room temperature down to 3K. The final version of the detector is now in production and will be commissioned at the end of 2011.

References

- [1] http://lmu.web.psi.ch/facilities/PSI-HighFieldMuSR/Project_Description.pdf, 2011.
- [2] E. Holzschuh. Direct measurement of muonium hyperfine frequencies in Si and Ge. *Phys. Rev. B*, 27:102, 1983.
- [3] K. Sedlak, R. Scheuermann, A. Stoykov, and A. Amato. GEANT4 simulation and optimisation of the high-field μ SR spectrometer. *Physica B*, 404:970–973, 2009.
- [4] A. Stoykov, R. Scheuermann, and K. Sedlak. A time resolution study with a plastic scintillator read out by a Geiger-mode Avalanche Photodiode. Submitted to Elsevier, 2011.
- [5] A. Stoykov, J. Rodriguez R. Scheuermann, K. Sedlaki, and A. Amato. High-Field μ SR instrument at PSI: detector solutions. To be published in the proceedings of the 12th International Conference on Muon Spin Rotation, Relaxation and Resonance on Physica B, 2011.
- [6] <http://www.hamamatsu.com>, September 2011.
- [7] <http://www.photonique.ch>, September 2011.

[8] <http://www.eljentechnology.com>, September 2011.

[9] <http://www.detectors.saint-gobain.com>, September 2011.

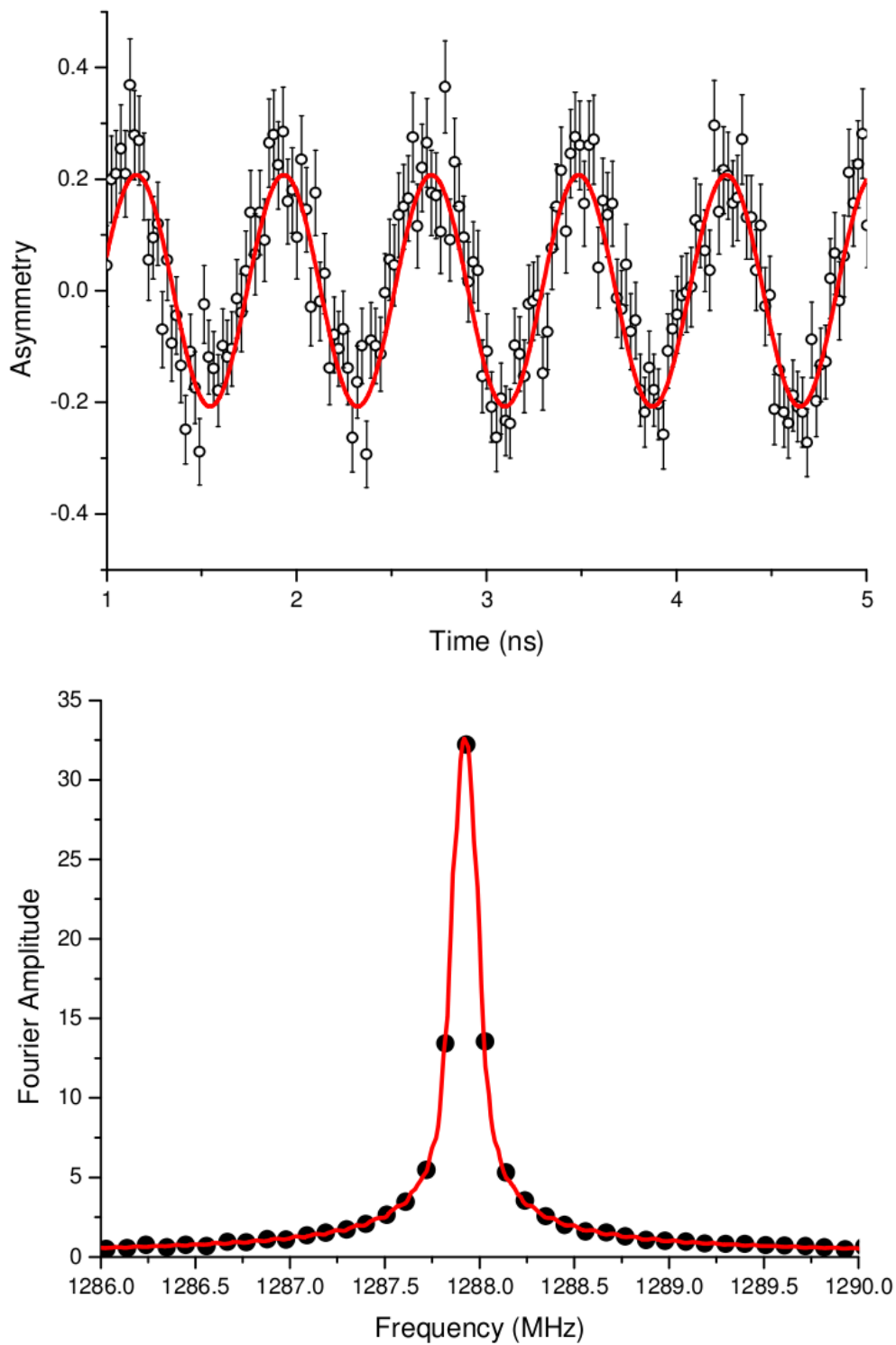


Figure 5: Top: Muon spin precession measured on a high purity silver sample in 9.5 T. Bottom: fast Fourier transform of this signal.

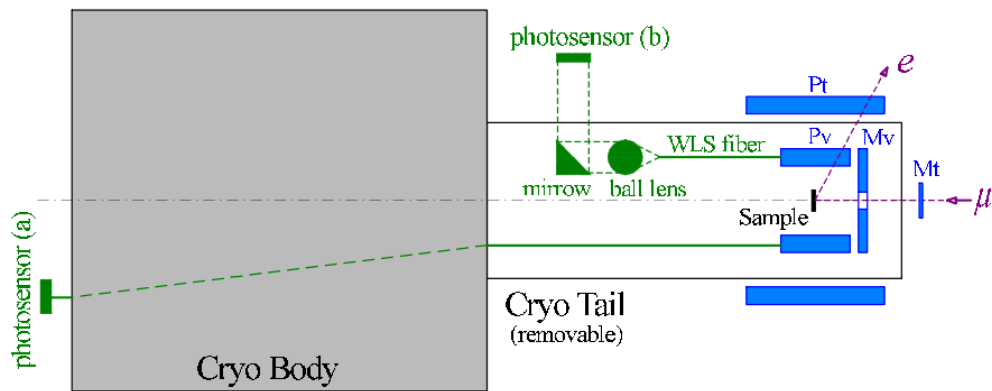


Figure 6: The sample environment and the detector layout of the DR. The sample is mounted on the cold finger of the DR. The radiation shields and the outer vacuum chamber in the tail part of the DR are removable to allow for sample change. Mt and Pt are the high time resolution muon and positron counters operated at room temperature. Mv and Pv are muon veto and positron validation counters: the scintillators with embedded wavelength shifting fibers are located in the vicinity of the sample on the 1 K radiation shield, the photosensors are at room temperature. The light from the scintillators will be transported to the G-APD by the optical array.

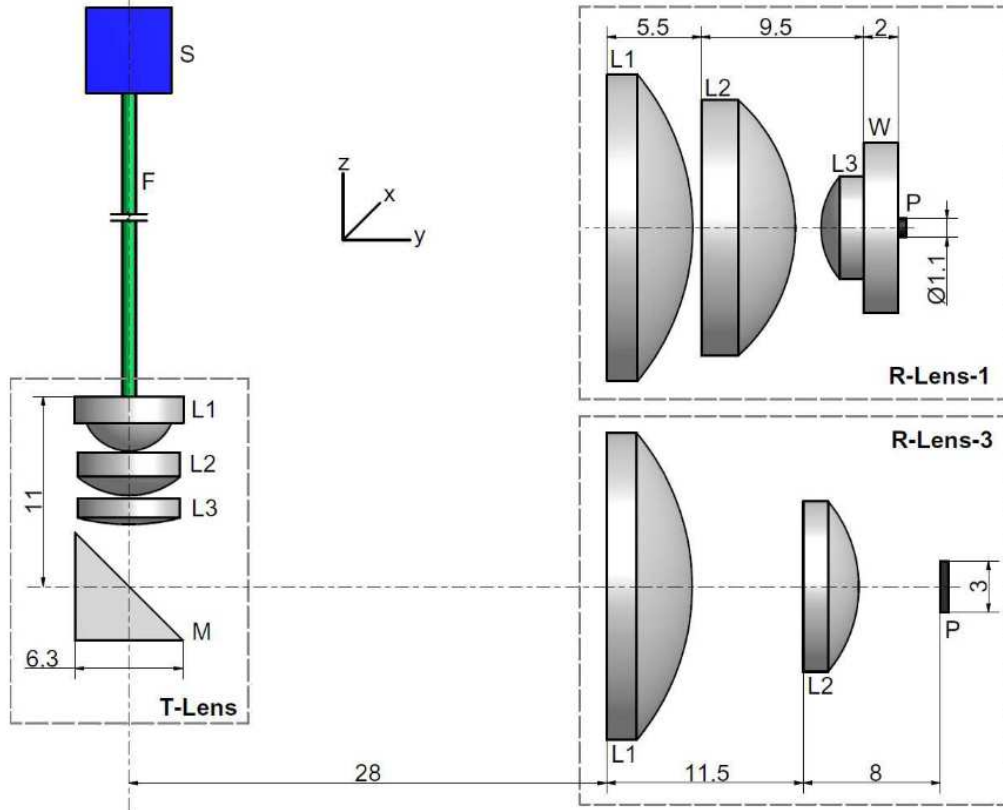


Figure 7: Scheme of light collection from the scintillator (S), via the WLS fiber (F) and the lens light guide (LLG), to the photosensor (P): S 5 mm thick EJ-204 plastic scintillator from Eljen [8] with a 1 mm deep groove to accommodate the fiber; F 0.8 mm multicladd BCF-92 WLS fiber from Bicon [9] glued into the scintillator using an Eljen EJ-500 optical cement; P photosensor. The transmitting T-Lens collects the light from the fiber and sends it to the receiving R-Lens, to be focused onto the G-APD. Depending on the active area of the photosensor, there are two versions of the R-Lens. The used optical components are listed below. T-Lens: L1 large numerical aperture aspherical lens ($NA = 0.62$), L2 plano-convex lens PCX 6x6, L3 PCX 6x24, M right-angle mirror; R-Lens-3: L1 PCX 18x18, L2 PCX 10x10; R-Lens-1: L1 PCX 18x18, L2 PCX 15x15, L3 PCX 6x6, W window 10 x 2 mm used as a spacer between the G-APD and the L3 lens. The window is glued to the G-APD with EJ-500 epoxy, and to the lens with a UV-light cured optical adhesive NOA-65 from Edmund Optics. The reason for gluing the window onto the G-APD is discussed in the text.

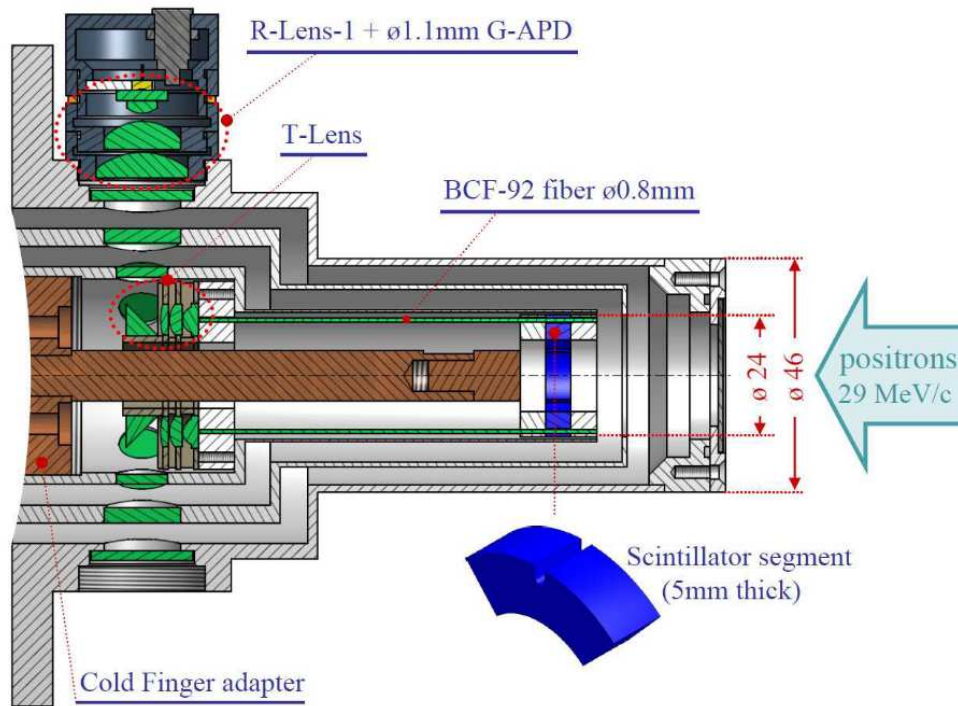


Figure 8: Design view of the cryostat tail part with build-in detector. The construction allows having up to 8 independent detector channels. The fibers are glued into the scintillators and the plexiglass supporting rings using EJ-500 epoxy. The T-Lens is assembled by stacking together component and spacing layers. Each component layer holds up to 8 identical optical elements arranged onto a circle: the lenses are glued into the corresponding holes using NOA-65 UV - cured optical adhesive, the mirrors are fixed with the Stycast epoxy.